Journal of Manufacturing Engineering, December 2025, Vol. 20, Issue. 4, pp 151-158
DOI https //doi.org/10.37255/jme.v20i4pp151-158

LOW-COST ESP32 ROBOTIC MAGNETOMETER FOR HIGH-RESOLUTION INDOOR MAGNETIC FIELD MAPPING

Gayan Gomus[1], Dushan Dinushka[2], Ashen Sannasgama[1] and Rangana Madushan[1]

[1]Department of Physics, University of Colombo, Colombo 00300, Sri Lanka
[2]Department of Electrical Technology, University College of Rathmalana, Rathmalana, Sri Lanka.

Abstract

Indoor magnetic fields are strongly distorted by building materials and electrical infrastructure, complicating magnetometer-based applications such as localisation and anomaly detection. We developed a low-cost, portable, ESP32-based three-axis magnetometer integrated on a small mobile robot to map indoor magnetic fields on a 10 cm × 10 cm grid. The robot followed predefined paths using infrared sensing, streamed measurements via Wi-Fi to a computer, and logged data to a Google Sheet for analysis. Spatial maps and contours were generated using Surfer to visualise field structure and variability. Field surveys were conducted in the Physics Department at the University of Colombo and compared against an outdoor baseline. Representative indoor corridor components reached X = 137.62 μT, Y = 261.98 μT, Z = 1.23 μT (resultant ≈ 296 μT), whereas outdoor measurements were X = 32.82 μT, Y = 23.09 μT, Z = 20.82 μT (resultant ≈ 45.2 μT). Contour maps reveal substantially greater spatial variation indoors than outdoors, with a resultant magnitude approximately 6.5 times higher at representative locations, indicating pronounced disturbances likely associated with structural metals and active wiring. These results demonstrate that a simple, reproducible robotic platform can produce high-resolution indoor magnetic cartography using commodity hardware, enabling rapid site assessment and supporting applications in magnetic fingerprinting, interference diagnosis, and infrastructure-free navigation.

Keywords: *Earth magnetic field, Indoor mapping, Magnetometer*

1. Introduction

The magnetic field is generated by electric currents resulting from the motion of convection currents in a mixture of molten iron and nickel in the Earth's outer core [1]. The magnitude of the Earth's magnetic field at its surface ranges from 25 to 65 μT (0.25 to 0.65 gauss) [2]. The North geomagnetic pole represents the South Pole of the Earth's magnetic field, and conversely, the South geomagnetic pole corresponds to the North Pole of the Earth's magnetic field [3]. Because opposite magnetic poles attract, and the north end of a magnet, like a compass needle, points toward the Earth's South magnetic field [4].

Magnetic field-line diagrams are a visualisation convention; when constructed with a uniform rule, the local line density is proportional to the field magnitude |B|, and the lines are everywhere tangent to |B|[5]. In iron filings demonstrations, the familiar banding arises because the external field induces dipole moments in the filings; the particles rotate and form chains along |B|, with their spacing and aggregation governed by particle size, aspect ratio, magnetic susceptibility, and inter-particle interactions, rather than by “like poles repelling” per se [6]. The geomagnetic field exhibits pronounced spatial eterogeneity and temporal variability; its strength and direction vary with location and evolve from seconds (magnetospheric/ionospheric disturbances) to years and decades (secular variation and geomagnetic jerks)[7]. Consequently, robust characterisation requires globally distributed measurements, combining satellite magnetometry with a network of approximately 200 permanent geomagnetic observatories, supplemented by temporary arrays for regional studies [6]. Indoors, magnetic field variability arises from ferromagnetic construction, magnetised objects, and time-varying currents in power distribution, motors, and electronic appliances. These sources generate both magnetostatic perturbations and alternating fields at mains frequency and its harmonics [6], [8]. The Earth's magnetic field, which is always pointed towards the north, has been used by humans from ancient times as a navigation aid. Within buildings, high-permeability structures distort and locally reorient the ambient field, so the measured direction need not coincide with magnetic north and the magnitude can be appreciably modified [9].

**Corresponding Author -E-mail: gayan2664@gmail.com*

Journal of Manufacturing Engineering, December 2025, Vol. 20, Issue. 4, pp 151-158
DOI https //doi.org/10.37255/jme.v20i4pp151-158

Time-varying magnetic fields induce electric fields in conductive media and thereby drive currents in the human body. Similarly, motion of a conductor through a static magnetic field generates induced currents via Faraday's law. [10]. Indoor magnetic-field signatures have attracted increasing attention in both academia and industry as a basis for localization, primarily because smartphone magnetometers are ubiquitous and low-cost [11]. A growing literature shows that geomagnetic anomalies can be exploited for accurate indoor positioning of pedestrians and mobile robots, often via fingerprinting or sequence-matching of magnetic measurements [12], [13]. In contrast to many conventional indoor localization approaches that depend on dedicated infrastructure such as Wi-Fi access points or BLE beacons, magnetic methods are inherently infrastructure-free and exhibit good temporal stability [14], [15]. Practically, these systems leverage the magnetometers embedded in commodity mobile phones, typically Hall-effect devices, to record ambient magnetic fields for navigation and tracking [16].

This project acquires and models the indoor magnetic vector field, producing a map of the measured signatures. Magnetic-field data were collected at specified locations using magnetoresistive sensors, and a robotic vehicle was built to evaluate the system. The processed measurements were visualised with Surfer 16 and GNU Octave. Surfer 16 is a scientific data-analysis and graphing package for Microsoft Windows [17], and it was used to generate contour maps from the collected and averaged magnetic-field magnitudes and directions at the surveyed locations.

2. Methodology

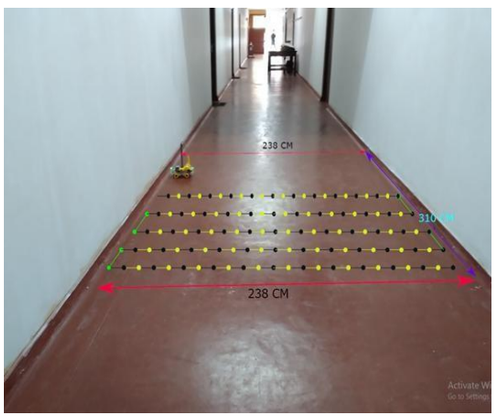

Fig. 1 Robotic car path, a square grid of about 10 cm x 10 cm distance at the department.

The magnetic fields are formed by stationary objects such as walls, concrete columns, steel railing, staircase, doorways, and electrical equipment inside a building. This project the main target was to control the robot car navigation path and collect the Earth's magnetic field data in the required places. It was in a square grid of about 10 cm x 10 cm. A robot car was a vehicle designed to capture magnetic fields in several places indoors using a magnetometer that was attached to the car, as shown in Fig. 1. ESP 32 is a series of low-cost. It has a low-power system on chip microcontrollers with integrated Wi-Fi and dual- mode Bluetooth. It has 520 KiB SRAM memory and 30

GPIO pins. A three-axis (X, Y, and Z directions) magnetometer sensor module was used to measure the direction and magnitude of the magnetic field within a building [18]. The HMC5883L magnetic sensor module was used to measure the three-axis components of the magnetic field in locations. It is based on Anisotropic magneto-resistive (ARM) technology with a small-sized chip and digital interface, which is designed to measure both direction and magnitude of the geomagnetic field from 8 milli gauss to 8 gauss. This chip also includes an integrated 12-bit ADC, a maximum data rate of 160 Hz, an I2C digital interface, and 1.2-degree heading accuracy [19]. The block diagram of the magnetic field mapping system is shown in Fig. 2.

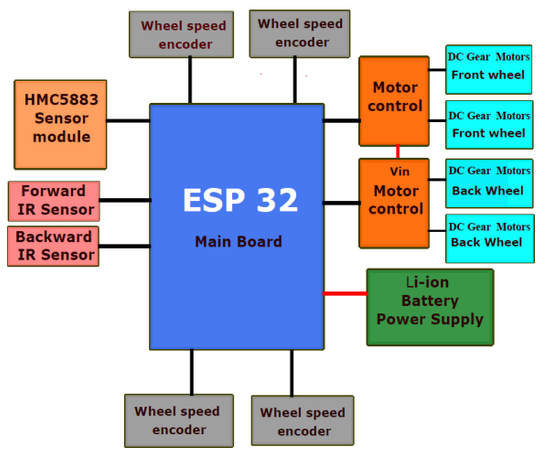

Fig. 2 The block diagram of the magnetic field mapping system

The mainboard mainly consists of an ESP32 Module. The ESP 32 Module was attached to all other parts of this circuit, as shown in Fig. 2 block diagram of the system above. The 5 V and 3.3 V regulator power supply was used for other sensor modules. The main

Journal of Manufacturing Engineering, December 2025, Vol. 20, Issue. 4, pp 151-158
DOI https //doi.org/10.37255/jme.v20i4pp151-158

power supply was a Li-ion rechargeable battery supply (18650). The HMC5883 sensor module was connected to the ESP32 module and obtained the x, y, and z magnetic field components. Two L298N DC motor controllers were used to control the four wheels of the robot vehicle in forward and backward directions.

2.1 Wheel direction

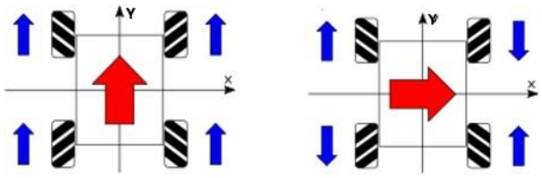

Fig. 3 Robotic car wheel direction [20]**.**

Every Mecanum wheel has free rollers, which make a 45-degree angle with the wheel's axis. The robot car can move in any direction. All four wheels move forward or backward in the same direction by rotating as shown in Fig. 3. By controlling the two wheels on one diagonal in the same direction and the other two wheels in the opposite direction, sideways movement is achieved, as shown in Fig. 2.3 (move right).

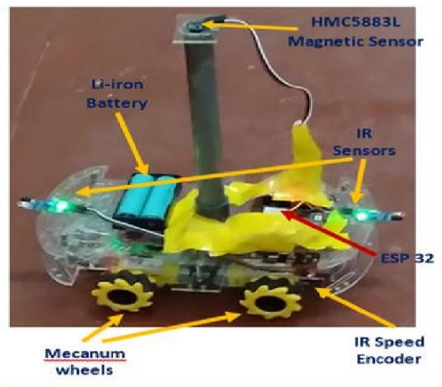

Fig. 4 Fully completed robotic car. The robot car was mainly built on an ESP32. The sensor providing magnetometer readings was mounted on the top. The reference location was provided by the physics department

At the starting point of navigation, the robotic car was programmed to move forward in a specified direction. The indoor magnetic field was recorded in ten datasets at a single location using a magnetometer sensor, with the measurements transmitted to a computer via Wi-Fi. These datasets were continuously uploaded and organised in tabular form using Google Sheets. The robotic car advanced in 10 cm increments, recording magnetometer readings at each position. When the infrared (IR) sensor detected a wall, the car shifted 10 cm to the left before reversing. The resulting navigation path of the car is illustrated in Fig. 1.

2.2 HMC5883 sensor module mounting

Proper sensor mounting is a critical requirement for the operation of this robotic system. The DC motors contain permanent magnets, and their operation produces magnetic fluctuations. In addition, electronic circuits inherently generate localised magnetic fields in the vicinity of circuit boards. As a result, sensor measurements may be affected by these interferences, reducing accuracy. To mitigate this issue, the robotic car was equipped with a 1-foot sensor mounting stand, on which the sensor was positioned to obtain more reliable readings.

3. Results and discussions

Experiments were performed at the Physics Department building at the University of Colombo. To estimate the magnetic field variations at various locations in the physics department, magnetic field measurements were taken continuously. The physics department building has long corridors with beams and a Staircase. The corridors are covered by a concrete slab and a concrete beam. A picture of a corridor on the first floor is shown in Fig. 5. Magnetic field data were collected by using a robotics car that was moved in the corridor, staircase, and lab. Out of the building, magnetic field data were collected. All magnetic field data were mapped using the contour mapping and 3D surface mapping techniques.

Fig. 5 Picture illustrating the first-floor corridor of the Physics department.

Journal of Manufacturing Engineering, December 2025, Vol. 20, Issue. 4, pp 151-158
DOI https //doi.org/10.37255/jme.v20i4pp151-158

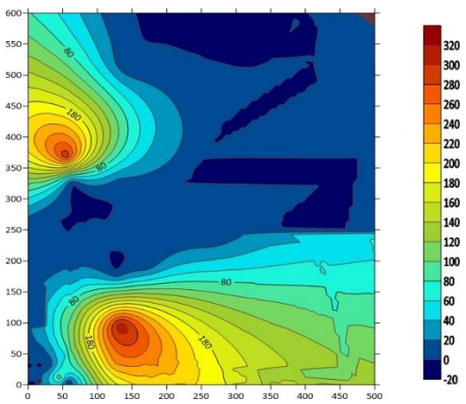

Fig. 6 Contour map in the first-floor corridor. The magnetic field was recorded under a concrete beam and between each wall on both sides of the corridor.

Fig. 6 shows the magnetic field variations in the first-floor corridor in the physics department building. The magnetic field was recorded under a concrete beam and between each wall on both sides of the corridor. This magnetic field varies between 0 μT and 320 μT. The typical shape of the magnetic field is depicted in Fig. 7. Darker reds represent a greater field presence, where darker blues signify a weaker field. The magnetic field intensity in the corridor is higher than that of the outdoor environment.

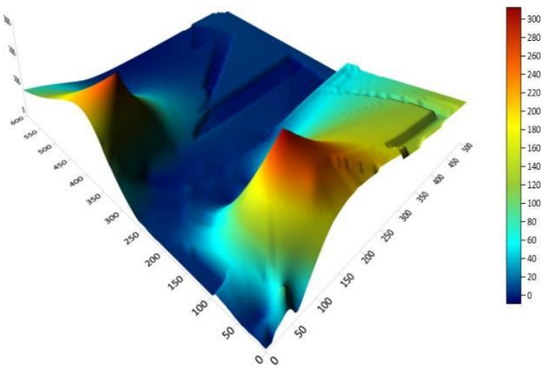

Fig. 7 Fig. 3.3 3D surface map in the first-floor corridor. Darker reds represent a greater field presence, where darker blues signify a weaker field.

3.1 Paper Heading

An AC current wire was dragged into this corridor area to change the magnetic field. It was connected to a 1500-watt Electrical Kettle. The robotic car navigated and began collecting magnetic field sensor readings in the corridor again. This is illustrated in Figs. 8 and 9.

Fig. 8 This picture shows the corridor where the AC wire line was dragged and connected to the electric kettle.

Fig. 9 The robotics car navigated and started to collect magnetic field sensor readings.

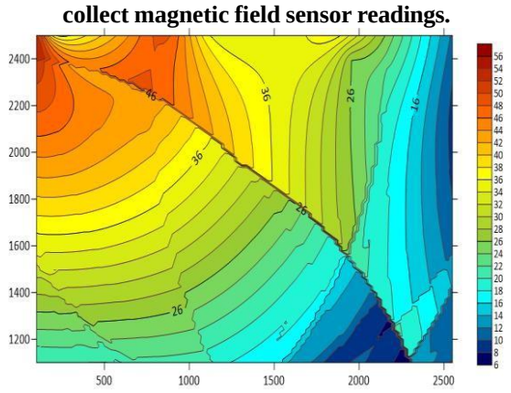

Fig. 10 Contour map showing the magnetic field intensities of the corridor that had dragged the AC wire area. Darker reds were represented for a greater magnetic field signifies an AC current wire area.

Journal of Manufacturing Engineering, December 2025, Vol. 20, Issue. 4, pp 151-158
DOI https //doi.org/10.37255/jme.v20i4pp151-158

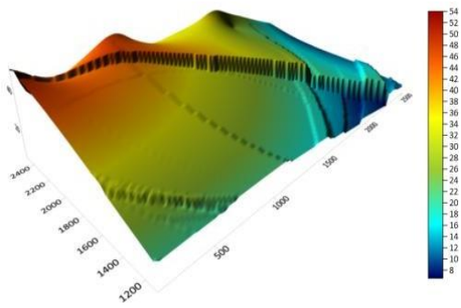

Fig. 11 3D surface map showing the magnetic field intensities of the corridor that had dragged the AC wire area. Where concrete beams and other disturbances in the blue colour in Fig. 6 changed to yellow and green.

The collected data were used to illustrate the variation in the magnetic field along the corridor with an AC current wire. This magnetic field varies between 0 μT and 60 μT. Darker reds were used to represent a greater magnetic field, which signifies an area with an AC current wire. Where concrete beams and other disturbances in the blue colour in Fig. 6 changed to yellow and green. At that time, the magnetic field intensity in the corridor had more variance than in the normal corridor.

3.2 The magnetic field effect of the DC wire line on the corridor.

The rheostat and wire are visible in Fig. 12. The collected data were used to illustrate the variation in the magnetic field along the corridor. This mapping is illustrated below (Fig. 12 and Fig. 13). The magnetic field affects the DC wire line in the corridor. It has been connected to the Rheostat. This magnetic field effect does not have more variance than the AC wire line effect. It was a little similar to the normal corridor effect.

Fig. 12 This picture has shown the corridor that had dragged the DC wire line connected to the rheostat.

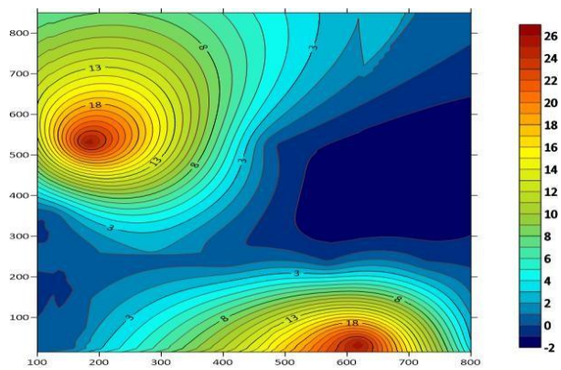

Fig. 13 Contour map showing the magnetic field intensities of the corridor that had dragged the DC wire area. This illustrates the same as Fig. 6 the magnetic field variation.

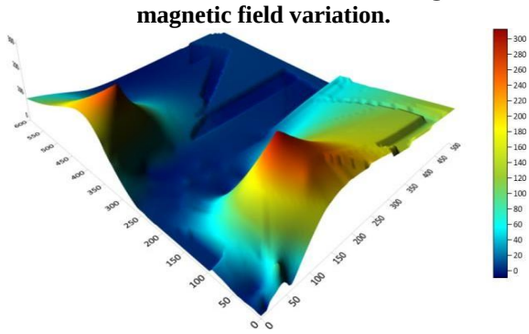

Fig. 14 3D surface map in the first-floor corridor. Darker reds represent a greater field presence, where darker blues signify a weaker field.

3.3 The magnetic field intensity variation in the computer lab.

This picture is in the computer lab in the physics department.

Fig. 15 Picture illustrating the computer lab area.

Journal of Manufacturing Engineering, December 2025, Vol. 20, Issue. 4, pp 151-158
DOI https //doi.org/10.37255/jme.v20i4pp151-158

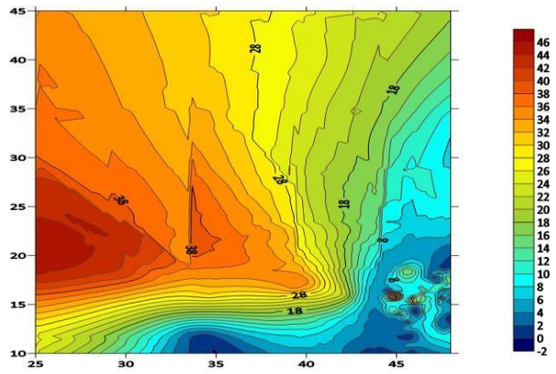

Fig. 16 Contour map in the computer Lab. showed the magnetic field variations in the computer lab. The aluminum door and partition were surrounded by the area.

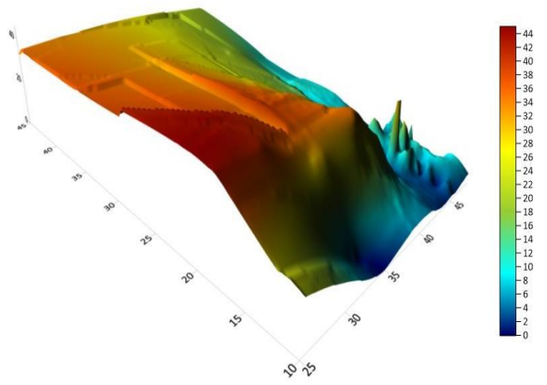

Fig. 17 3D surface map in the computer Lab. This illustrates that darker red and orange colours were fully used in the computer lab. Magnetic field variations were higher than in a corridor.

Fig. 16 shows the magnetic field variations in the computer lab. The aluminium door and partition were surrounded by the area. This illustrates that darker red and orange colours were fully used in the computer lab. Magnetic field variations were higher than in a corridor. The variance of the robotic car navigation distance error is larger than that of the staircase. Because the variation of the location in the computer lab is a large distance as shown in Fig. 15.

3.4 The magnetic field intensity variation in the staircase.

The Department Staircase is shown in this picture.

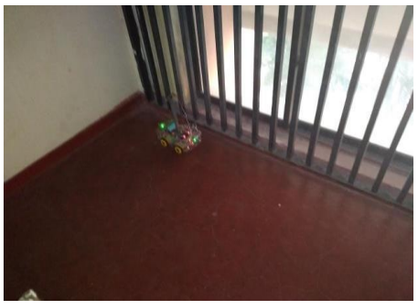

Fig. 18 : Picture illustrating the staircase of the physics department

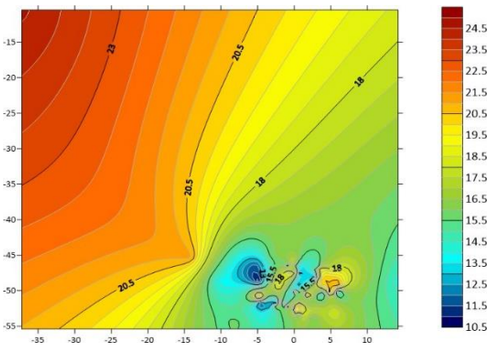

Fig. 19 : Contour map in the staircase. Department staircase magnetic field variations were the same as those in the computer lab.

Department staircase magnetic field variations were the same as those in the computer lab. A lot of ferromagnetic objects have a round shape. This illustrates that darker red was a variation of a very high value. The variance of the magnetic field intensity was larger, making it difficult to distinguish between true and false positions.

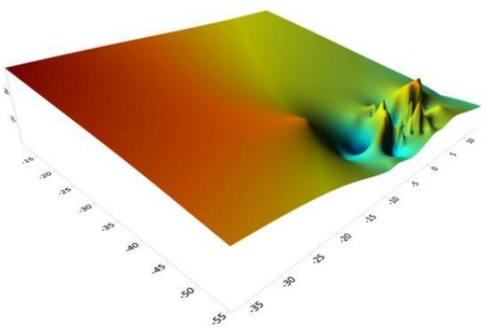

Fig. 20: 3D surface map in the staircase. This illustrates that darker red was a variation of a very high value.

Journal of Manufacturing Engineering, December 2025, Vol. 20, Issue. 4, pp 151-158
DOI https //doi.org/10.37255/jme.v20i4pp151-158

3.5 The magnetics filed variation in the outside of the building.

Experiments were performed outside in the building to check variation without disturbance for the magnetic field. This magnetic field variation was significantly smaller than the indoor magnetic field variations observed in the contour maps. The yellow color has more area on this map. The orange and green colors have mixed with yellow color. So it could be shown as more stable than the indoor field. The dark red and dark blue colors have small areas on the map. The variance of the magnetic field intensity is small. The outdoor magnetic field was no a disturbance-free area. So the magnetic field is everywhere and relatively stable. Fig. 22 and Fig, 23 maps are very useful to compare for the indoor magnetic field intensity.

Fig. 21 : Picture illustrating the outside of the physics department building

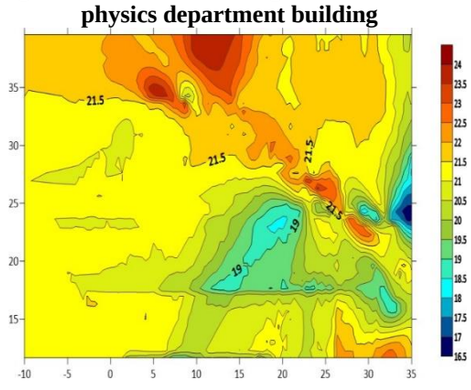

Fig. 22 : Contour map Outside the physics department building

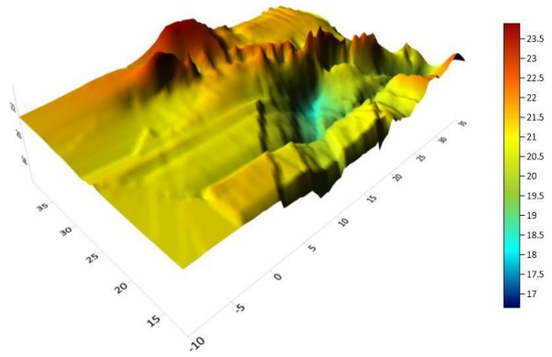

Fig. 23 : 3D surface in Outside of the physics department building

4. Conclusions

In this project, the magnetic field anomalies for indoor within the building were investigated using mobile robotic car navigation. According to the contour map, obtaining from the collected data significant magnetic field anomalies were observed near the concrete beam at the corridor, staircase, and lab. These disturbances are induced by metallic structures present in most buildings. Locations with high magnetic fields due could be identified by mapping the magnetic field variations inside a building. It can be affected by nearby magnetic fields generated by sources such as the ringing of a mobile phone near the sensor and other magnetic field generating instruments. When the ferromagnetic material objects were moving in the environment where the experiment was being carried out, magnetic field measurements can be changed unexpectedly. In mechanical construction of the robotic car was done to minimize slipping and rolling over when it was moved. The magnetic field mapping system will be necessary to collect the magnetic field data (x, y, z component) at different times at the buildings for further development.

Acknowledgment

I want to thank my supervisor Dr. M. K. Jayananda for his guidance, monitoring, and constant encouragement throughout this Project. I also want to express my gratitude to my advisors Dr. Hiran Jayaweera and Dr. Lakmal Weerawarne for their guidance. Of course, friends and family are important as well. I am grateful to my friends and family. I am thankful to Mr. CMP Perera and Mr. Upendra Lakshan of the Department of Physics, the University of Colombo.

Journal of Manufacturing Engineering, December 2025, Vol. 20, Issue. 4, pp 151-158
DOI https //doi.org/10.37255/jme.v20i4pp151-158

Reference

1. *"Origin of Earth's Magnetic Field, Its Nature and Behavior, Geophysical Consequences, and Danger to Humanity: A Logical Progression of Discoveries—A Review," Advances in Image and Video Processing, vol. 10, no. 6, Dec. 2022, doi: 10.14738/aivp.106.13684.*
2. *"The Earth's Magnetic Field: An Overview," Geomagnetism, British Geological Survey. [Online]. Available: http://www.geomag.bgs.ac.uk/*
3. *M. Regi, D. Di Mauro, and S. Lepidi, "The location of the Earth's magnetic poles from circum-terrestrial observations," J. Geophys. Res.: Space Physics, vol. 126, no. 2, Feb. 2021, doi: 10.1029/2020JA028513.*
4. *S. K. Runcorn, "The Earth's magnetism," Philosophical Transactions of the Royal Society of London, vol. 193, no. 3, pp. 152–163, 1955, doi: 10.2307/24944764.*
5. *"4466_Preview_Contents."*
6. *C. Rizos, Proceedings of the 2012 International Conference on Indoor Positioning and Indoor Navigation (IPIN), Sydney, Australia, Nov. 13–15, 2012. Piscataway, NJ, USA: IEEE, 2012.*
7. *B. Heilig, C. Beggan, and J. Lichtenberger, "Natural sources of geomagnetic field variations," CERN—European Organization for Nuclear Research, 2018.*
8. *J. A. Malik, "Impact of heavy metals from building and constructive materials on aquatic environment," in Springer Tracts in Civil Engineering. Cham, Switzerland: Springer, 2021, pp. 275–292, doi: 10.1007/978-3-030-57418-5_10.*
9. *Z. Wu, M. Wen, G. Peng, X. Tang, and D. Wang, "Magnetic-assisted initialization for infrastructure-free mobile robot localization," arXiv:1911.09313, Nov. 2019. [Online]. Available: http://arxiv.org/abs/1911.09313*
10. *K. Zhu and A. Kiourti, "A review of magnetic field emissions from the human body: Sources, sensors, and uses," IEEE Open Journal of Antennas and Propagation, 2022, doi: 10.1109/OJAP.2022.3186643.*
11. *G. Ouyang and K. Abed-Meraim, "A survey of magnetic-field-based indoor localization," Electronics, vol. 11, no. 6, Mar. 2022, doi: 10.3390/electronics11060864.*
12. *N. Yu, X. Chen, R. Feng, and Y. Wu, "High-precision pedestrian indoor positioning method based on inertial and magnetic field information," Sensors, vol. 25, no. 9, May 2025, doi: 10.3390/s25092891.*
13. *L. Fernandes et al., "An infrastructure-free magnetic-based indoor positioning system with deep learning," Sensors, vol. 20, no. 22, pp. 1–19, Nov. 2020, doi: 10.3390/s20226664.*
14. *G. Ouyang, K. Abed-Meraim, and Z. Ouyang, "Magnetic-field-based indoor positioning using temporal convolutional networks," Sensors, vol. 23, no. 3, Feb. 2023, doi: 10.3390/s23031514.*
15. *J. Dai, M. Wang, B. Wu, J. Shen, and X. Wang, "A survey of latest Wi-Fi assisted indoor positioning on different principles," Sensors, Sep. 2023, doi: 10.3390/s23187961.*
16. *Y. Cai, Y. Zhao, X. Ding, and J. Fennelly, "Magnetometer basics for mobile phone applications," Electronic Products.*
17. *Golden Software, "Surfer®: Powerful contouring, gridding, and surface mapping system—Full user's guide." [Online]. Available: www.GoldenSoftware.com*
18. *randomnerdtutorials, "Getting started with the ESP32 development board." [Online]. Available: https://randomnerdtutorials.com/getting-started-with-esp32/*
19. *Honeywell, "3-axis digital compass IC HMC5883L." [Online]. Available: www.honeywell.com*
20. *Wikipedia, "Mecanum wheel.".*